Journal Pre-proof

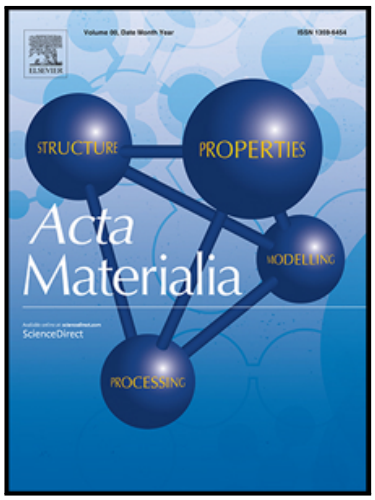

Surprising increase in yield stress of Mg single crystal using long-period stacking ordered nanoplates

Koji Hagihara , Ryohei Ueyama , Michiaki Yamasaki , Yoshihito Kawamura , Takayoshi Nakano

PII: S1359-6454(21)00177-4
DOI: https://doi.org/10.1016/j.actamat.2021.116797
Reference: AM 116797

To appear in: *Acta Materialia*

Received date: 23 September 2020
Revised date: 7 January 2021
Accepted date: 6 March 2021

Please cite this article as: Koji Hagihara , Ryohei Ueyama , Michiaki Yamasaki , Yoshihito Kawamura , Takayoshi Nakano , Surprising increase in yield stress of Mg single crystal using long-period stacking ordered nanoplates, *Acta Materialia* (2021), doi: https://doi.org/10.1016/j.actamat.2021.116797

Surprising increase in yield stress of Mg single crystal using long-period stacking ordered nanoplates

Koji Hagihara[1*], Ryohei Ueyama[1], Michiaki Yamasaki[2],
Yoshihito Kawamura[2], Takayoshi Nakano[1]

[1]Division of Materials and Manufacturing Science, Graduate School of Engineering, Osaka University, 2-1 Yamadaoka, Suita, Osaka 565-0871, Japan.
[2]Magnesium Research Center & Department of Materials Science, Kumamoto University, 2-39-1 Kurokami, Chuo-ku, Kumamoto 860-8555, Japan.
[*]**Corresponding author:** E-mail: hagihara@mat.eng.osaka-u.ac.jp, Tel: +81668797434

Abstract

Mg–Zn–Y ternary alloys containing the long-period stacking ordered (LPSO) phase exhibit superior mechanical properties. This is believed to be originating from the LPSO phase acting as the strengthening phase. However, we first clarify that the mechanical properties of the matrix Mg solid solution in the Mg/LPSO two-phase alloy are significantly different from those of pure Mg. The yield stress of a $Mg_{99.2}Zn_{0.2}Y_{0.6}$ single crystal (matrix Mg solid solution) is almost the same as that of an LPSO single-phase alloy. This is ascribed to the formation of thin stacking-fault-like defects, named “LPSO nanoplate”. In $Mg_{99.2}Zn_{0.2}Y_{0.6}$, kink-band formation is induced in the same manner as that in the LPSO phase in deformation, resulting in high strength accompanied with increased ductility. Our results suggest that the strengthening mechanism of the Mg/LPSO two-phase alloy must be reconsidered depending on the microstructure. Furthermore, the results suggest that new ultrahigh-strength Mg alloys, which have much lower Zn and Y contents but the mechanical properties are comparable or superior than the present Mg/LPSO two-phase alloys, are expected to be developed via the appropriate control of LPSO nanoplate microstructures.

Keywords: Mg alloy; strength; LPSO-phase; microstructure; nanoplate

1. Introduction

There is an increased demand for the development of new lightweight structural materials to overcome issues related to global warming. Mg alloys are a potential candidate for addressing these issues. However, there are serious drawbacks for expanding the use of Mg alloys in many fields of application—notably, their insufficient strength and low corrosion resistance. Commercial cast Mg alloys exhibit a low tensile yield strength of ÿ100–250 MPa and limited ductility (elongation: 3%–15%) at room temperature [1]. In order to improve these properties, Mg alloys containing the long-period stacking ordered (LPSO) phase have recently received attention [2–15]. The LPSO phase is known to form in Mg–Zn–Y ternary alloys. The LPSO phase has an approximate composition of Mg–5at% Zn–7at% Y in the typical Mg/LPSO two-phase alloy with a composition of $Mg_{97}Zn_1Y_2$. The crystal structure of the LPSO phase is constructed by the long-period stacking—typically, 18- or 14-fold—of close-packed planes (the basal plane in hexagonal systems) along the *c* axis [16,17]. Additionally, the Y/Zn atoms in the LPSO phase are periodically segregated into four specific layers of close-packed planes where a face-centered cubic (fcc)-like stacking fault exists [17], as illustrated in Supplementary Fig. S1. Kawamura et al. first reported that a rapidly solidified Mg/LPSO two-phase alloy with a composition of $Mg_{97}Zn_1Y_2$, which contains the ~24 vol% of LPSO phase, exhibits an extremely high yield stress of ~600 MPa while retaining ~5% elongation [2]. Further, a high ultimate tensile strength of ~400 MPa can be obtained for extruded alloys fabricated by a simpler process [5]. To clarify the physical origin of this drastic strengthening, the mechanical properties of the LPSO phase have been extensively studied. Hagihara et al. examined the mechanical properties of the LPSO phase by using a directionally solidified (DS) LPSO single-phase crystal [18–20]. As a result, the plastic deformation behavior of the LPSO phase was found to have strong anisotropy. Basal slip can be operative in the LPSO phase, similar to Mg, and is

accompanied by a low yield stress. However, in the case where stress is applied parallel to the basal plane, the yield stress is quite high and different from that in Mg; this is because the formation of deformation twins is prohibited, which is ascribed to the complicated LPSO structure [18]. Instead, unique kink bands are formed, resulting in ductility [18–20]. A kink band is a deformation band in which basal dislocations are aligned along a direction perpendicular to the slip plane [18–25], as illustrated in Supplemental Fig. S2. More recently, it was found that the formed kink bands act as effective obstacles to the motion of basal dislocations, contributing to the strengthening of the LPSO phase (kink-band strengthening) [26,27].

In contrast, the mechanical properties of the matrix Mg phase in Mg/LPSO two-phase alloys have not received as much attention from researchers. The composition of the Mg matrix phase [3] is approximately Mg–0.2at% Zn–0.6at% Y. The mechanical properties of Mg–Y and Mg–Zn binary alloys were examined by some researchers using single crystals [28–31]. However, the effects of the coaddition of Zn and Y on the mechanical properties have not received significant attention until now. In this study, we used a single crystal prepared by directional solidification to ascertain the effects of coaddition. We found that the mechanical properties of the Mg solid solution are entirely different from those of pure Mg and similar to those of the LPSO phase, which we report here in detail. Moreover, the physical origin of the drastic increase in yield stress is discussed.

2. Experimental procedure

A master ingot with a composition of Mg–0.2at% Zn–0.6at% Y was prepared by induction melting in a carbon crucible. Directional solidification was conducted using the Bridgman technique (Nissin Giken NEV-DS2) in an Ar-gas atmosphere at a growth rate of 5.0 mm/h. The microstructure of the obtained DS crystal was examined by optical microscopy (OM; Olympus BX51M), laser microscopy (LM; Olympus DSX510), scanning electron microscopy (SEM; JEOL JSM-7800F) at 15 kV, and transmission electron microscopy (TEM; JEOL JEM-3010) at 300 kV. Furthermore, the distribution of

Zn/Y atoms was examined by high-angle annular dark-field scanning transmission electron microscopy (HAADF-STEM; JEOL JEM-2100F) at 200 kV. In addition to the as-DS-grown crystals, the microstructure observation was conducted to some heat-treated specimens. As the first condition, some as-DS-grown specimens were annealed at 520 °C for 5 h under Ar atmosphere, followed by water quenching. As the second condition, the specimen annealed at 520 °C was further annealed at 400 °C for 5 h, followed by water quenching. Then, the variations in microstructure in them were examined by abovementioned methods.

For comparison of the deformation behavior, pure-Mg single crystals were also grown by the same method at a growth rate of 10.0 mm/h. From the microstructural analyses, the obtained DS crystal was confirmed to consist of some large grains of the Mg solid solution phase with a diameter of ~ 5–8 mm. From the large grains, single-crystal rectangular specimens with dimensions of 2 × 2 × 5 mm^3 were cut for compression tests by electrodischarge machining. The crystal orientation of the specimen was determined by X-ray backscatter Laue diffraction analysis.

Four different crystal orientations were selected as loading axes in the compression tests to examine the orientation dependence of the plastic deformation behavior. The four orientations correspond to [0001], [01$\bar{1}$0], [11$\bar{2}$0], and [1 1 $\bar{2}$ 1.85], as indicated in the stereographic projection in Fig. 2(a), later. The Schmid factors for the possible deformation modes for the four loading axes that were expected from reports on the deformation behavior of pure Mg and its solid solutions [28–38] are listed in Supplemental Tables S1 and S2. Before the compression tests, specimens were mechanically polished using emery paper and then chemically polished in an ethanol–20-vol% nitric acid solution to remove surface damage. Compression tests were performed at a nominal strain rate of 1.67×10^{-4} s^{-1} at temperatures ranging from RT (~20 °C) to 400 °C using universal testers (Shimadzu AG-5kNX System, and Instron 8862 System), in vacuum. The influence of the heat-treatment to the deformation behavior was also examined by the compression test using the abovementioned

heat-treated specimens at [$11\bar{\varsigma}0$] at RT.

In addition, some tensile tests were conducted to examine the ductility of the as-DS-grown single crystal. The tensile tests were conducted by using the plate-like specimens with the gauge dimension of 2 × 1 mm^2 × 5 mm, along [0001] orientation at RT, in vacuum.

Deformation markings placed on specimen surfaces were analyzed using OM with Nomarski interference contrast, and the operative deformation mode was determined. The variation in the crystal orientation due to deformation was examined by electron backscatter diffraction (EBSD) pattern analysis in the SEM at a measured step distance of 1.0 μm. During the preparation of specimens for SEM-EBSD, a specimen's surface was mechanically polished using emery paper, and a final treatment was conducted using a cross-section polisher (JEOL IB19500CP). The deformation microstructure was further examined by TEM. Specimens for TEM observation were prepared by ion milling using Ar (Fishione Model 1051 TEM Mill,).

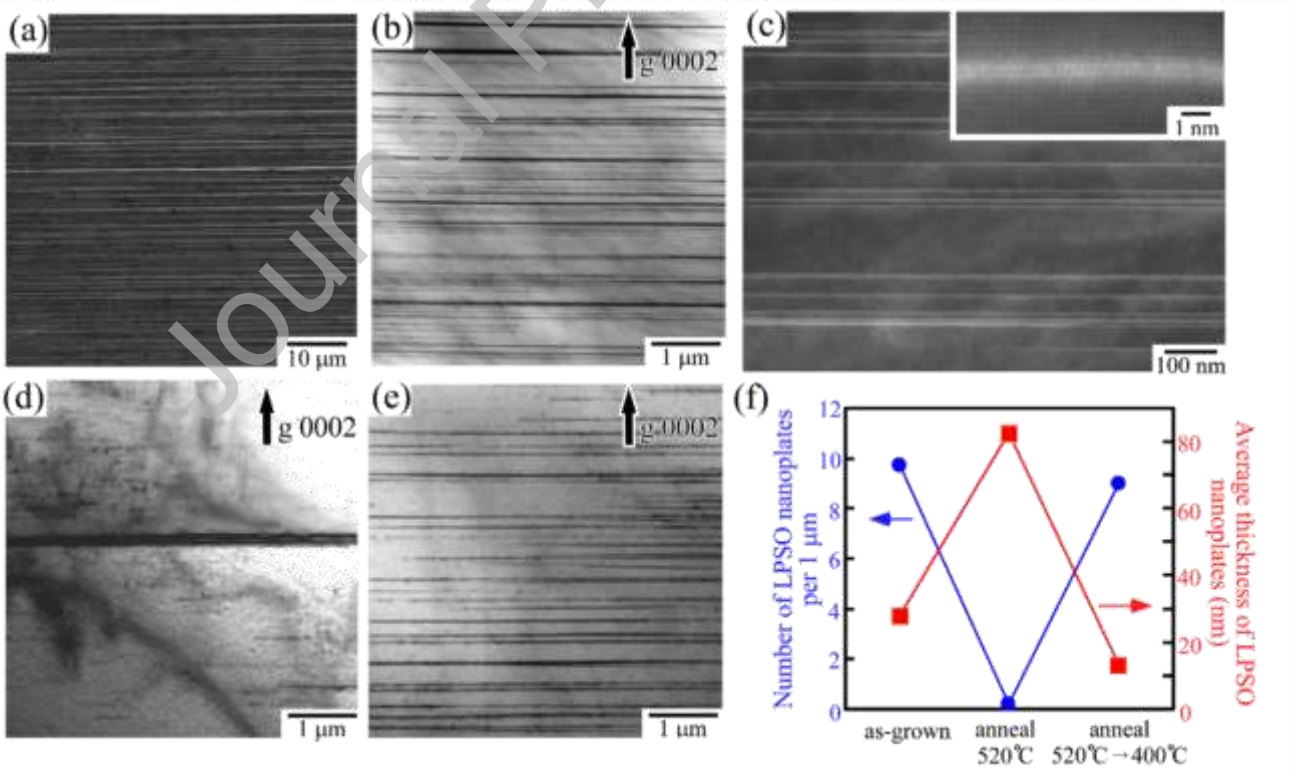

Fig. 1 *(a) SEM image of the as-grown DS alloy. (b) Bright-field TEM image showing the microstructure in the as-grown alloy. (c) Corresponding HAADF-STEM image. The inset*

Y. T. Zhu, S. N. Mathaudhu, Ultrastrong Mg alloy via nano-spaced stacking faults, Mater. Res. Lett. 1 (2013) 61-66.

[49] H. Pan, Q. Huang, G. Qin, H. Fu, M. Xu, Y. Ren, J. She, B. Song, B. Li, Activations of stacking faults in the calcium-containing magnesium alloys under compression, J. Alloys Comp. 692 (2017) 898-902.

[50] H. Wang, H. Geng, D. Zhou, K. Niitsu, O. Muransky, D. Zhang, Multiple strengthening mechanisms in high strength ultrafine-grained Al–Mg alloys, Mater. Sci. Eng. A 771 (2020) 138613

[51] M. Ana, Q. Denga, Y. Lia, H. Song, M. Su, J. Cai, Molecular dynamics study of tension-compression asymmetry of nanocrystal a-Ti with stacking fault, Mater. Design 127 (2017) 204–214.

[52] R. Su, D. Neffati, J. Cho, Q. Li, J. Ding, H. Wang, Y. Kulkarni, X. Zhang, Phase transformation induced plasticity in high-strength hexagonal close packed Co with stacking faults, Scripta Mater. 173 (2019) 32–36.

[53] K. Hagihara, T. Nakano, K. Sasaki, Anomalous strengthening behavior of Co–Cr–Mo alloy single crystals for biomedical applications, Scripta Mater. 123 (2016) 149-153.

[54] K. Hagihara, K. Hayakawa, K. Miyoshi, Inducement of kink-band formation in directionally solidified Mg/$Mg_{17}Al_{12}$ eutectic alloy - Inspired by the deformation behavior of the long-period stacking ordered (LPSO) phase, Mater. Sci. Eng. A 798 (2020) 140087.

[55] http://www.mfs-materials.jp/en/

Additional information

Supplementary Information accompanies this paper.

(4 figures and 2 tables are included.)

Figure captions

Fig. 1 (a) SEM image of the as-grown DS alloy. (b) Bright-field TEM image showing the microstructure in the as-grown alloy. (c) Corresponding HAADF-STEM image. The inset shows a higher-magnification image. Zn/Y atoms are segregated along four atomic layers where an fcc-type stacking fault exists. (d, e) TEM images showing the variation in microstructure due to heat treatment: (d) specimen in Fig.1(b) was annealed at 520 °C for 5 h followed by water quenching, and (e) specimen in Fig.1(d) was annealed further at 400 °C for 5 h. (f) Variation in the number of LPSO nanoplates per 1 μm and their average thickness according to heat treatment, measured along [0001] in the TEM. The observation direction is parallel to $[11\bar{2}0]$ in all the Figs. 1(a–e).

Fig. 2 (a) Temperature dependence of the yield stress of the as-grown $Mg_{99.2}Zn_{0.2}Y_{0.6}$ single crystal in four loading orientations. The yield stress of the pure-Mg single crystals reported in ref. [32] and that measured in this study are also plotted in gray for comparison. (b, c) Typical stress–strain curves deformed at (b) RT and (c) 300 °C in four different loading orientations.

Fig. 3 OM images showing the deformation traces in specimens deformed at RT. Specimens were deformed to ~5% plastic strain in the loading orientations of (a, b) $[1\ 1\ \bar{2}\ 1.85]$, (c, d) $[11\bar{2}0]$, (e, f) $[01\bar{1}0]$, and (g, h) [0001]. The Miller indices of the side surface planes in observation are indicated at the top-right corner in the images.

Fig. 4 Macroscopic views showing the variations in the deformation microstructure with temperature. Specimens were deformed in the (a) $[11\bar{2}0]$ and (b) $[01\bar{1}0]$ loading orientations to ~5% plastic strain at the temperatures indicated. The Miller indices of the side surface planes in observation are indicated in the figure.

Fig. 5 (a, b) Crystal orientation maps of deformation microstructures of the specimen

deformed in the [11$\bar{\varsigma}$0] orientation at RT to ~5% plastic strain and observed on the (1$\bar{\rho}$00) side surface. (c, d) Distributions of the crystal rotation angle in the deformation bands with respect to the matrix (undeformed region), measured in the regions around Fig. 5(a) and (b), respectively. (e) Crystal orientation map of the specimen deformed in the [01$\bar{\rho}$0] orientation at RT to ~5% plastic strain and observed on the ($\bar{\varsigma}$110) side surface. (f) The same region in Fig. 5(e), but the colors in the map indicate the crystal orientation along the loading axis, in order to distinguish the orientation colors of the deformation twins and deformation kink bands. (g) Distribution of the crystal rotation angle in the region around Fig. 5(e). The colors of the bar graph of Figs. 5(c), (d), and (g) indicate the crystal rotation axis of the measured bands: blue: near <$\bar{\varsigma}$110> and green: near <1$\bar{\rho}$00> with a deviation-angle tolerance of 10°. (h) Schematic showing the definitions of the crystal rotation angle and crystal rotation axis in the deformation band.

Fig. 6 (a) Bright-field TEM image of the deformation kink bands introduced in the specimen deformed in the [11$\bar{\varsigma}$0] orientation at RT to ~5% plastic strain. The observation direction is nearly parallel to [1$\bar{\rho}$00] in the matrix. (b) Higher-magnification image of the kink bands. (c–f) SAED patterns taken at points A–D indicated in Fig. 6(b).

Fig. 7 (a) Temperature dependencies of the CRSS estimated in the as-grown $Mg_{99.2}Zn_{0.2}Y_{0.6}$ single crystal investigated in this study, and (b) those in pure-Mg single crystals reported in refs. [33-35] and measured in this study.

Fig. 8 (a) Variation in the yield stress with heat treatment for deformation in the [11$\bar{\varsigma}$0] orientation at RT. (b, c) Macroscopic views of the deformation microstructure in specimens (b) annealed at 520 °C for 5 h, and (c) annealed further at 400 °C for 5 h, prior to compression tests. The side surface planes in observation are parallel to (0001).

Fig. 9 Comparison of yield stresses of the as-grown $Mg_{99.2}Zn_{0.2}Y_{0.6}$ single crystal and

LPSO phase. The yield stresses of the $Mg_{99.2}Zn_{0.2}Y_{0.6}$ single crystal are indicated by the red points. In addition, the DS 18R-LPSO phase previously reported in ref. [20] are indicated by the gray points.

Fig. 10 (a) Stress-strain curve in the tensile test of $Mg_{99.2}Zn_{0.2}Y_{0.6}$ single crystal along [0001] at RT. The entire view of the deformed specimen is inserted in the figure. (b) Higher magnification image of the deformation microstructure showing the formation of many deformation kink bands, observed at the part indicated by the red circle in Fig. 10(a). *The side surface planes in observation is parallel to* $(10\bar{1}0)$.

Declaration of interests

☒ The authors declare that they have no known competing financial interests or personal relationships that could have appeared to influence the work reported in this paper.

☐The authors declare the following financial interests/personal relationships which may be considered as potential competing interests:

Graphic Abstract

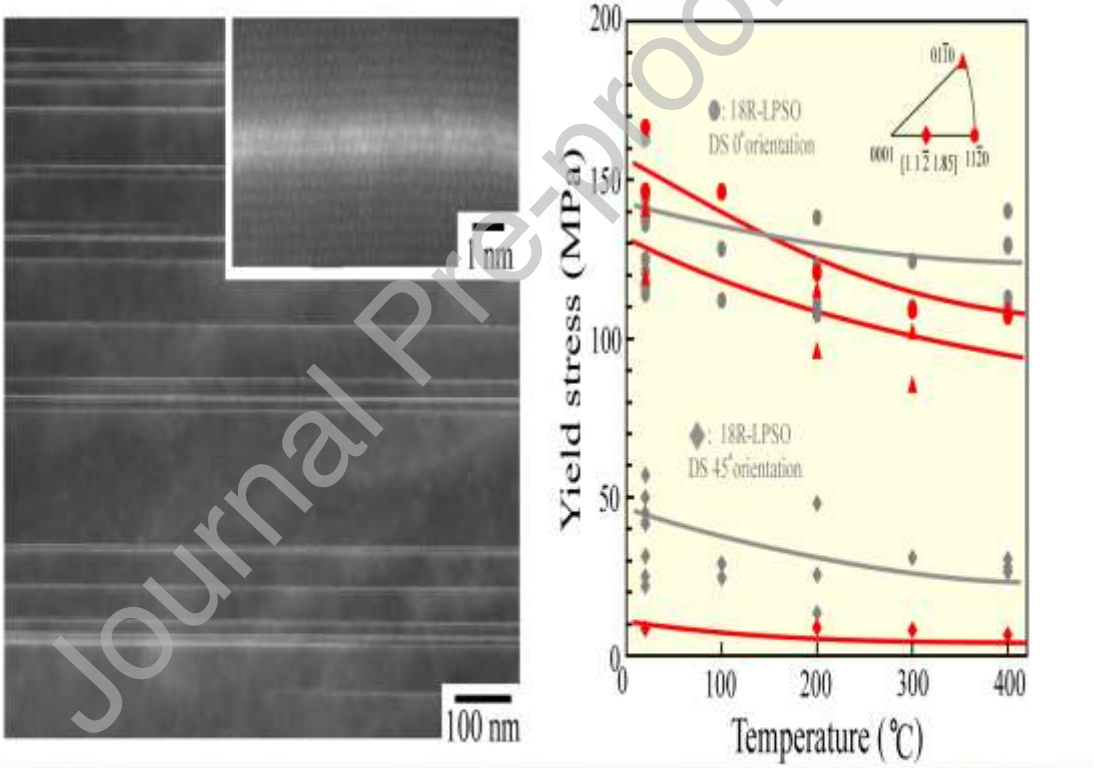

"LPSO nanoplate" strengthens the Mg phase, whose yield stress is comparable to the bulk LPSO-phase